Atmos. Chem. Phys., 16, 9349–9359, 2016
www.atmos-chem-phys.net/16/9349/2016/
doi:10.5194/acp-16-9349-2016

Atmospheric Chemistry and Physics Open Access EGU

Speciation of OH reactivity above the canopy of an isoprene-dominated forest

J. Kaiser[1,a], K. M. Skog[1], K. Baumann[2], S. B. Bertman[3], S. B. Brown[4,5], W. H. Brune[6], J. D. Crounse[7], J. A. de Gouw[4,5,8], E. S. Edgerton[2], P. A. Feiner[6], A. H. Goldstein[9,10], A. Koss[4,8], P. K. Misztal[9], T. B. Nguyen[7], K. F. Olson[9], J. M. St. Clair[7,b,c], A. P. Teng[7], S. Toma[3], P. O. Wennberg[7,11], R. J. Wild[4,8], L. Zhang[6], and F. N. Keutsch[12]

[1]Department of Chemistry, University of Wisconsin-Madison, Madison, WI, USA
[2]Atmospheric Research & Analysis Inc, Cary, NC, USA
[3]Department of Chemistry, Western Michigan University, Kalamazoo, MI, USA
[4]Chemical Sciences Division, NOAA Earth System Research Laboratory, Boulder, CO, USA
[5]Department of Chemistry, University of Colorado, Boulder, CO, USA
[6]Department of Meteorology, Pennsylvania State University, University Park, PA, USA
[7]Division of Geological and Planetary Sciences, California Institute of Technology, Pasadena, CA, USA
[8]Cooperative Institute for Research in Environmental Sciences, University of Colorado Boulder, Boulder, CO, USA
[9]Department of Environmental Science, Policy, and Management, University of California, Berkeley, CA, USA
[10]Department of Civil and Environmental Engineering, University of California, Berkeley, CA, USA
[11]Division of Engineering and Applied Science, California Institute of Technology, Pasadena, CA, USA
[12]School of Engineering and Applied Sciences and Department of Chemistry and Chemical Biology, Harvard University, Cambridge, MA, USA
[a]now at: School of Engineering and Applied Sciences, Harvard University, Cambridge, MA, USA
[b]now at: Joint Center for Earth Systems Technology, University of Maryland Baltimore County, Baltimore, MD, USA
[c]now at: Atmospheric Chemistry and Dynamics Laboratory, NASA Goddard Space Flight Center, Greenbelt, MD, USA

Correspondence to: J. Kaiser (jkaiser@seas.harvard.edu)

Received: 11 December 2015 – Published in Atmos. Chem. Phys. Discuss.: 18 January 2016
Revised: 12 July 2016 – Accepted: 12 July 2016 – Published: 28 July 2016

Abstract. Measurements of OH reactivity, the inverse lifetime of the OH radical, can provide a top–down estimate of the total amount of reactive carbon in an air mass. Using a comprehensive measurement suite, we examine the measured and modeled OH reactivity above an isoprene-dominated forest in the southeast United States during the 2013 Southern Oxidant and Aerosol Study (SOAS) field campaign. Measured and modeled species account for the vast majority of average daytime reactivity (80–95 %) and a smaller portion of nighttime and early morning reactivity (68–80 %). The largest contribution to total reactivity consistently comes from primary biogenic emissions, with isoprene contributing $\sim$60 % in the afternoon, and $\sim$30–40 % at night and monoterpenes contributing $\sim$15–25 % at night. By comparing total reactivity to the reactivity stemming from isoprene alone, we find that $\sim$20 % of the discrepancy is temporally related to isoprene reactivity, and an additional constant $\sim 1\,s^{-1}$ offset accounts for the remaining portion. The model typically overestimates measured OVOC concentrations, indicating that unmeasured oxidation products are unlikely to influence measured OH reactivity. Instead, we suggest that unmeasured primary emissions may influence the OH reactivity at this site.

1 Introduction

Biogenic emissions of volatile organic compounds (VOCs) constitute the largest source of reactive carbon in the atmosphere (Guenther et al., 2012). During the daytime, oxida-

tion of VOCs by the OH radical can drive the formation of secondary pollutants. Under high NO_x ($NO + NO_2$) conditions, peroxy radicals (RO_2) generated from VOC oxidation convert NO to NO_2, which ultimately photolyzes to form ozone. Additionally, oxidized VOCs (OVOCs) are typically less volatile than their precursors and can contribute to the formation of secondary organic aerosol (SOA). Therefore, it is important to understand the total VOC + OH reaction rate and the fate of the resultant OVOC to understand the formation of tropospheric ozone and SOA.

While measuring every VOC and oxidation product is not feasible, measurement of OH reactivity (the loss rate of the OH radical divided by the OH concentration) provides an alternative to the bottom–up molecular approach (Kovacs and Brune, 2001). The absolute value of OH reactivity can be used to estimate the total amount of reactive carbon in an air mass or the RO_2 production rate. The speciation of the reactivity carries air-quality-relevant implications as SOA yield is directly tied to molecular properties such as volatility, hygroscopicity, viscosity, and condensed-phase reactivity.

One half of the annual non-methane VOC emissions is in the form of isoprene (C_5H_8), making it the dominant biogenic VOC globally (Guenther et al., 2012). Due to isoprene's abundance and high reactivity, the chemistry of isoprene and its resulting oxidation products have been the focus of numerous field studies. OH reactivity has been examined in four isoprene-dominated forests, with some studies suggesting missing primary emissions or missing OVOCs and others finding good agreement between measurements and calculations.

In a deciduous forest in Northern Michigan, DiCarlo et al. (2004) could account for only 50 % of the OH reactivity measured above the canopy in the summer of 2000. As OVOCs calculated by a model did not significantly increase calculated OH reactivity and as the missing reactivity fit a terpenoid-like emission profile, unmeasured terpene emissions were cited as a large source of reactive carbon in this environment. However, later measurements of monoterpenes and sesquiterpenes at this site suggested that only ∼ 20 % of the missing reactivity could be attributed to these primary VOCs (Kim et al., 2009). Additionally, Kim et al. (2011) found that measurements and calculations of OH reactivity in branch enclosures of isoprene-emitting trees at the same site were in good agreement. Using measurements taken at this site during 2009, Hansen et al. (2014) found that isoprene accounted for 60–70 % of afternoon OH reactivity both within and above the forest canopy. Because in-canopy OH reactivity calculations and measurements were in good agreement, the authors concluded that there are unlikely to be unmeasured primary VOCs at this site. However, above-canopy comparisons show a large missing fraction of reactivity, suggesting that unmeasured oxidation products may contribute at longer processing times.

In a downy oaks forest in the Mediterranean southeast of France, Zannoni et al. (2016) examined OH reactivity both within and above the canopy. Measured and calculated OH reactivity were in good agreement at both heights during the daytime, with isoprene contributing 83 % within the canopy and 74 % above the canopy. However, more than 50 % of nighttime reactivity was missing on a subset of days. The authors conclude that unmeasured, higher-generation isoprene oxidation products account for part of the nighttime discrepancy, alongside unmeasured OVOCs produced from the ozonolysis of large, non-isoprene biogenic VOCs.

In a tropical rainforest in Borneo, unmeasured isoprene-derived OVOCs were a more dominant contribution to the observed reactivity than isoprene itself, at nearly 50 % (Edwards et al., 2013). OH reactivity measured from a clearing atop a hill surrounded by forest was significantly underestimated by a model (∼ 60 % at noon). The authors concluded missing that primary emissions were unlikely to contribute significantly to OH reactivity, and an underrepresentation of secondary multifunctional OVOCs is a likely source of discrepancies.

Finally, in the tropical rainforest of Suriname, in-canopy OH reactivity measured could not be reached by summing the contributions from measured isoprene, methyl-vinyl ketone, methacrolein, acetone, and acetaldehyde. The authors called for a more comprehensive measurement suite to investigate the large discrepancy (65%) (Sinha et al., 2008).

Each forest examined in these studies is composed of a unique mixture of tree species, potentially leading to different relative contributions of non-isoprene primary emissions. Furthermore, different meteorological conditions and canopy structures may lead to different processing times and resultant contributions of isoprene-derived OVOCs. While these differences may make the above studies difficult to generalize, they all address an underlying question: are isoprene-derived OVOCs a substantial source of missing reactive carbon? If so, after what degree of processing?

To assess the contribution of unmeasured oxidation products, ideally, one would explicitly model all isoprene OVOCs and include modeled species in the summation. Additionally, several OVOC measurements would be available to test the reliability of model concentrations. This sort of analysis has been performed in a chamber study of the oxidation of isoprene (Nölscher et al., 2014), but as initial concentrations of reactants were orders of magnitude greater than those found in the atmosphere, and as physical processes such as deposition onto plant surfaces are not captured in chamber studies, chamber experiments may not capture the behavior of OH reactivity observed in a forest. Of the above field studies, several rely only on the concentration of measured species in the calculation of OH reactivity (Sinha et al., 2008; Hansen et al., 2014 (part 2 will include a modeling study); Zannoni et al., 2016). While studies that employ model OVOC concentrations have a more complete representation of oxidation products (DiCarlo et al., 2004; Edwards et al., 2013), neither of these studies compare measured and modeled OVOC mixing ratios. Additionally, as isoprene hydroxyl hydroperox-

ide (ISOPOOH) and isoprene hydroxy nitrate (ISOPN) standards have only recently become available (Rivera-Rios et al., 2014; Lee et al., 2014), first-generation oxidation product measurements are often incomplete.

With high isoprene emissions, the southeast United States is an ideal location to reassess questions of missing OH reactivity and speciation of observed reactivity. In addition to measurements of OH reactivity, the 2013 Southern Oxidant and Aerosol Study (SOAS) field campaign provides a comprehensive suite of VOC and OVOC measurements, enabling a more constrained analysis of the contribution from isoprene-derived OVOCs than previously available. This includes first-generation isoprene oxidation products for both low-NO and high-NO oxidation, such as ISOPOOH, ISOPN, isoprene hydroperoxy aldehydes (HPALD), and the sum of methyl-vinyl ketone (MVK) and methacrolein (MACR), as well as several smaller oxidation products. Furthermore, dry-deposition rates of isoprene's OVOCs are measured and parameterized for this site (Nguyen et al., 2015), enabling us to reduce some of the uncertainty related to physical losses of carbon. Speciated and total monoterpene measurements provide additional insight into reactive carbon not stemming from isoprene.

Using a 0-D box model, we investigate the sources of reactive carbon and compare the summation of calculated species with measured OH reactivity. We then discuss our findings in the context of previous studies and briefly discuss the air-quality-relevant implications. Further discussion on the isoprene oxidation mechanism and product formation can be found in Su et al. (2016) and Xiong et al. (2015), and modeled OH and HO_2 are discussed more fully in Feiner et al. (2016).

2 Methods

2.1 SOAS measurements

Measurements were performed from 1 June to 15 July at the SouthEastern Aerosol Research and CHaracterization (SEARCH) Centreville (CTR) site near Brent, Alabama, as part of the 2013 SOAS field campaign (http://soas2013.rutgers.edu/). CTR is a rural site surrounded by mixed deciduous-evergreen forests, at times experiencing urban influence from Birmingham, Montgomery, or Tuscaloosa, AL. The long-term and regional chemical tends observed at this site have been discussed in detail elsewhere (Blanchard et al., 2013; Hidy et al., 2014). We restrict our analysis to the time frame of good instrumental overlap (11 June to 16 July 2013). All observations shown here are binned to 30 min time intervals. A discussion of missing data interpolation can be found in the Supplement.

Table 1 summarizes the chemical measurements used in this analysis and their related uncertainties. Most chemical measurements and solar radiation were acquired from a walk-up tower with a height of ~ 20 m, approximately 10 m above the forest canopy. CO, gas chromatograph–electron capture detector (GC-ECD) measurements, and meteorological parameters (relative humidity, temperature, pressure, and boundary layer height) were acquired from a nearby trailer.

Key measurements to this analysis are OH reactivity, VOCs, and OVOCs. OH reactivity was measured by adding OH to an airstream using a moveable wand and monitoring the decay of the OH radical by laser-induced fluorescence (Mao et al., 2009). The instrument zero ($4.3\,s^{-1}$) is determined by measuring the wall loss of the OH radical while using a clean carrier gas. The uncertainty in the zero is $0.5\,s^{-1}$, with 2σ confidence. The recycling of OH from $HO_2 + NO$ was corrected by taking into account measured HO_2 decays. The accuracy of the instrument was verified using gasses with well-known reaction rate coefficients (C_3F_6 in the field, and CO, propane, propene, and isoprene in the lab). Further details about the operating procedures for the OH reactivity instrument are described in Mao et al. (2009).

Most VOCs were measured by gas chromatography-mass spectrometry (GC-MS), which provided 5 min samples every 30 min (Gilman et al., 2010). Due to possible line losses for oxygenated species in GC-MS measurements, proton-transfer reaction time-of-flight mass spectrometry (PTR-TOFMS, Ionicon Analytik model PTR-TOF 8000) measurements are used for the sum of MVK and MACR (Jordan et al., 2009). The PTR-TOFMS also provided measurements of the total monoterpene mixing ratio. Unspeciated monoterpenes are defined as the difference between the PTR-TOFMS measurement of total monoterpenes and the sum of individual species measured by the GC-MS (α-pinene, β-pinene, limonene, myrcene, and camphene).

Glycolaldehyde, ISOPOOH, and isoprene dihydroxy epoxides (IEPOX) were measured by CF_3O^- triple quadrupole chemical ionization mass spectrometry (Paulot et al., 2009; St. Clair et al., 2010, 2014). ISOPN, HPALD, the sum of MVK and MACR nitrates ($MACNO_3 + MVKNO_3$), hydroxyacetone, and peroxyacetic acid were measured by chemical ionization time-of-flight mass spectrometry (Crounse et al., 2006; Lee et al., 2014). Formaldehyde (HCHO) was measured by fiber-laser-induced fluorescence (Hottle et al., 2008; DiGangi et al., 2011), and glyoxal was measured by laser-induced phosphorescence (Huisman et al., 2008). Additional speciated organic nitrates were measured by a gas chromatography–electron-capture detector (Roberts et al., 2002).

2.2 Model simulations

A 0-D box model analysis was performed using the University of Washington Chemical Box Model (UWCM) (Wolfe and Thornton, 2011), incorporating the Master Chemical Mechanism, MCM v3.2 (Jenkin et al., 1997; Saunders et al., 2003; website: http://mcm.leeds.ac.uk/MCM), updated to include the isoprene alkyl radical-O_2 adduct equilibria

Table 1. SOAS measurements used in this study.

Instrument	Parameters[a]	1σ uncertainty	Reference or model number
OH laser-induced fluorescence	OH[b] OH reactivity	16 % (30 min) 10 % (30 s)	Mao et al. (2009)
Tropospheric Airborne Chromatograph for Oxy-hydrocarbons	VOCs[b]	20 % (30 min)	Gilman et al. (2010)
Proton-transfer-reaction time-of flight mass spectrometer	Total monoterpenes[b]	20 % (1 min)	Jordan et al. (2009)
	MVK + MACR	40 % (1 min)	
CF_3O^- triple quadrupole chemical ionization mass spectrometry	ISOPOOH, IEPOX, Glycolaldehyde	100 ppt + 70 % (0.5 s)	St. Clair et al. (2010)
Fiber-laser-induced fluorescence	HCHO	15 % (1 s)	Hottle et al. (2008); DiGangi et al. (2011)
Madison laser-induced-phosphorescence	Glyoxal	9 % (1 s)	Huisman et al. (2008)
Gas chromatograph–electron capture detector	PAN[c], PPN[d], MPAN[e]	20 % (20 min)	Roberts et al. (2002)
CF_3O^- compact time-of-flight mass spectrometer	HCOOH[b], H_2O_2[b], HNO_3[b], ISOPN, Hydroxyacetone, Peroxyacetic acid, HPALD, $MACNO_3 + MVKNO_3$	100 ppt + 30–50 % (5 s)	Crounse et al. (2006)
Absorption of IR with gas filter correlation	CO[b]	7.4 % (5 min)	Thermo Scientific Model 48i-TLE
Nitrogen oxides by cavity ring down	O_3[b]	3 % (1 min)	Fuchs et al. (2009); Wild et al. (2014)
	NO[b]	8 % (1 min)	
	NO_2[b]	3 % (1 min)	

[a] All species listed are constrained when calculating OH reactivity. [b] Denotes species constrained when calculating both OH reactivity and OVOC mixing ratios. [c] Peroxyacetyl nitrate. [d] Peroxypropionyl nitrate. [e] Methacryloyl peroxynitrate.

(Peeters and Müller, 2010), isoprene peroxy radical isomerizations (Crounse et al., 2011; da Silva et al., 2010), revised ISOPOOH + OH rate constant (St. Clair et al., 2015), and HPALD photolysis and OH reaction rates (Wolfe et al., 2012). Monoterpene reactions for species not included in the MCM (i.e., myrcene, camphene, and unspeciated monoterpenes) are described in Wolfe et al. (2011). At each time step, photolysis rates are scaled according to the ratio of measured radiation and the maximum observed radiation at that time of day.

Dry deposition is included for H_2O_2, organic hydroperoxides, nitrates, and the isoprene-derived epoxides (IEPOX). Measured deposition velocities are used for H_2O_2, IEPOX, and ISOPN. For other hydroperoxides and organic nitrates, noontime deposition velocities are calculated according to the relationship with mass shown by Nguyen et al. (2015). Diurnal variability of deposition velocities are scaled according to the measured variation for representative species (ISOPOOH for peroxides, methacrolein nitrate for nitrates).

Dilution is assumed to occur with air with a concentration of zero for all species. This dilution represents entrainment with free tropospheric air and any decrease in concentrations related to unrepresented deposition or advection processes. A constant, empirically determined rate of 4 day^{-1} is used in all analysis presented here, giving a 6 h lifetime with respect to dilution. A sensitivity analysis of this dilution rate is provided in Sect. 3.2. The model is initiated with a 2-day spin-up period using diurnal averages of measured species to account for the buildup of unmeasured intermediate species.

Two separate model configurations are used to examine OH reactivity and OVOC concentrations. In all discussions of modeled OH reactivity, OVOC concentrations are constrained to their measurements to ensure the most complete representation of measured OH reaction partners. This includes constraining ISOPN, ISOPOOH, MVK + MACR, $MVKNO_3 + MACNO_3$, HPALD, and IEPOX by applying modeled isomeric distributions to measured concentrations. Due to the partial conversion of ISOPOOH to

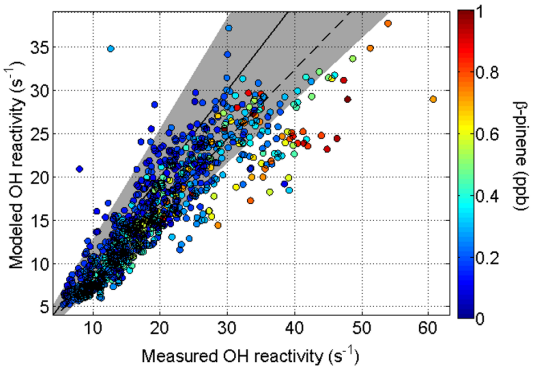

Figure 1. Comparison of measured and modeled OH reactivity colored by measured β-pinene concentrations. The solid line represents 1 : 1 agreement, and the dashed line ($y = 0.80x + 0.36$) represents the linear least squares fit weighted by uncertainty (York et al., 2004; Thirumalai et al., 2011). The gray shaded area represents the region with 28 % uncertainty of 1 : 1 agreement.

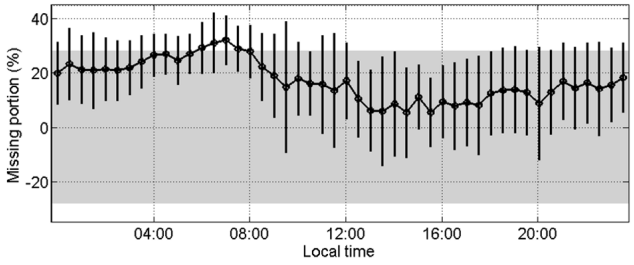

Figure 2. Diurnal profile of the discrepancy between measured and modeled OH reactivity. Error bars represent 1σ standard deviation of diurnal variability. Points in the gray shaded area are within the range of agreement considering combined measurement and model uncertainty (±28 %).

MVK + MACR in the PTR-TOFMS inlet (Rivera et al., 2014), this represents an upper limit on MVK and MACR measurements. However, because daytime ISOPOOH concentrations are a factor of > 5 lower than MVK + MACR and because the sensitivity to ISOPOOH is only ~ 30 % of that of MVK + MACR, the effect of ISOPOOH on the MVK + MACR signal is expected to be negligible. It should be noted that all species that react with OH are included in the calculated reactivity, whereas species that immediately regenerate OH as a reaction product (such as ISOPOOH + OH → IEPOX + OH) would not contribute to measured OH reactivity. The average total contribution from such species to calculated reactivity is small ($0.6 \pm 0.3\ s^{-1}$). The scenario for comparing modeled and measured OVOCs is identical, except that OVOCs are not constrained. Because OVOC concentrations are calculated in a separate model scenario, any discrepancy between measured and modeled OVOC concentrations does not translate to a discrepancy in calculated reactivity.

In both model configurations, OH, NO, NO_2, CO, O_3, H_2O_2, HNO_3, and all primary VOCs are constrained to their measurements. Primary VOCs are defined as any species that are likely to have a significant contribution from direct emissions. This includes alkanes, alkenes, aromatic compounds, and some oxygenated species (methanol, ethanol, acetone, methyl-ethyl-ketone, acetaldehyde, biacetyl, propanal, hydroxyacetone, and formic acid). Table 1 provides a listing of constraints for each model scenario.

Figure S5 in the Supplement provides model results for HO_x (HO_2 + OH), OH reactivity, and two first-generation OVOCs given a variety of possible constraints on HO_x and OVOCs. The result essential to this analysis is that model HO_x is in good agreement with measurements and has a minimal impact on calculated OH reactivity and model OVOC concentrations. Our results are in agreement with Feiner et al. (2016), which also employs a 0-D box model and the MCM isoprene oxidation mechanism. Feiner et al. (2016) provide a detailed discussion of the observed and modeled radical budget, which is beyond the scope of this manuscript.

3 Results

3.1 Measured and modeled OH reactivity

Figure 1 shows a comparison between measured and modeled OH reactivity for the constrained-OVOC scenario. Modeled and measured values are well correlated ($r^2 = 0.85$), with a slope of 0.80 ± 0.02. The average missing reactivity for all measurement points is 16 ± 18 %. An uncertainty of 20 % is assigned to model reactivity based on the uncertainty in isoprene, which comprises the majority of modeled reactivity. Propagating measurement uncertainty (20 %) and model uncertainty (20 %) yields at least 28 % uncertainty in the missing fraction of OH reactivity. As both the slope and average discrepancy agree with measurement within 28 %, on average, we find no significant discrepancy between modeled and measured OH reactivity. A subset of points that correspond to high β-pinene concentrations fall outside of this range. Most of these points occur early in the measurement period, from 11 to 17 June. To investigate the sources of these discrepancies, we examine both the diurnal variability and composition of OH reactivity.

Figure 2 shows the diurnal variability of the missing portion of reactivity. In the afternoon, the model typically captures > 90 % of OH reactivity. At night, the model typically captures ~ 80 % of measured reactivity. Early morning discrepancies show the largest average discrepancies, reaching an average of 32 % missing reactivity at 07:00 LT.

The average diurnal speciation of observed reactivity is shown in Fig. 3. Primary biogenic VOCs make up the largest fraction of modeled OH reactivity throughout the entire day, with isoprene contributing ~ 60% in the afternoon and ~ 30–40 % at night and monoterpenes contributing ~ 15–25 % at night. Oxygen-containing VOCs contribute less significantly

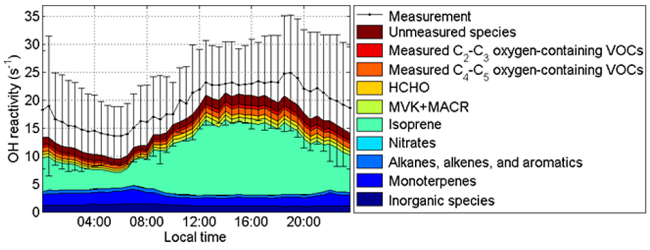

Figure 3. Diurnal profile of measured and modeled OH reactivity. Error bars represent 1σ standard deviation of diurnal variability.

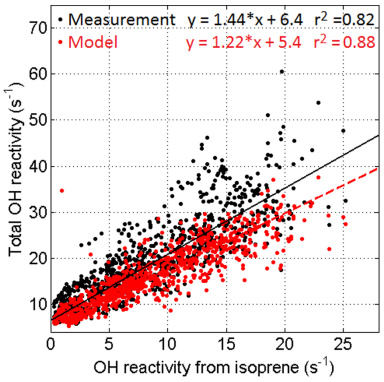

Figure 4. Total measured and modeled OH reactivity as a function of the OH reactivity calculated from isoprene alone. Lines represent least square linear fits weighted by uncertainty (York et al., 2004; Thirumalai et al., 2011) for measured (solid) and model (red dashed) OH reactivity.

at all time points (∼ 20–28 %), and the largest individual contributors are measured species such as HCHO (∼ 3–4 %), MVK, and MACR (∼ 2–4 %). Unmeasured oxidation products contribute ∼ 6–10 % of total modeled reactivity and are most prominent at night.

As discussed in Edwards et al. (2013), the increase in total reactivity with increase in isoprene is another useful parameter when considering OH reactivity speciation. In a plot of total OH reactivity plotted against the contribution from isoprene alone, the slope is related to the contribution from short-lived isoprene-derived OVOCs and VOCs co-emitted with isoprene. Figure 4 shows this relationship for measured and modeled OH reactivity, still referring to the OVOC-constrained scenario. Both observed and modeled OH reactivity are tightly correlated with OH reactivity from isoprene ($r^2 \geq 0.81$). The difference between model (1.22 ± 0.02) and observed (1.44 ± 0.02) slope is small but significant. This amounts to 15 % of reactivity correlated with isoprene reactivity not captured by measured species or modeled unmeasured oxidation products. The y intercept from measurements ($6.4 \pm 0.1\ s^{-1}$) and model (5.4 ± 0.1) also shows a small but significant difference. This indicates a missing reactivity of $\sim 1\ s^{-1}$ that is temporally distinct from isoprene reactivity.

3.2 Measured and modeled OVOCs

By investigating the model's ability to capture measured OVOC concentrations, we can assess the likely accuracy of model predictions of unmeasured species. As the model is constrained to measured OVOC concentrations when calculating model OH reactivity, the contribution of unmeasured species to total reactivity will be different in these two scenarios. However, the evaluation of model performance can be extended to the constrained-OVOC scenario.

Figure 5 shows the model's prediction of several measured OVOC concentrations. Isoprene's first-generation oxidation products MVK + MACR, ISOPOOH, ISOPN, and HPALD are overpredicted in the afternoon. Though the uncertainties in each of these measurements is large (40–70 %), all model concentrations are much higher than measurements. The model overestimates daytime HPALD observations by a factor of ∼ 6, ISOPOOH by a factor of ∼ 4, and ISOPN by a factor of ∼ 3. This translates to an overprediction of IEPOX and $MACNO_3 + MVKNO_3$, which are formed in the oxidation of ISOPOOH and ISOPN, respectively. For MVK + MACR, the daytime overprediction is approximately a factor of 2. Daytime agreement for MPAN, which is formed from MACR, is comparatively good. In general, smaller oxidation products (i.e., glyoxal, glycolaldehyde, and HCHO) are less susceptible to overprediction.

In an investigation of isoprene photochemistry and turbulent mixing during this campaign, the mixed layer chemical model (MXLCH) predicts similarly high values for ISOPOOH (1.5 ppb), MVK + MACR (3.0 ppb), and ISOPN (80 ppt) in the convective mixed boundary layer (Su et al., 2016). The MXLCH MVK + MACR mixing ratios are substantially higher than ground-based measurements but comparable to measurements from the Long-EZ research plane flying at altitudes of 100–1000 m a.g.l.

Model OVOC concentrations are highly sensitive to the assumed dilution scheme. This sensitivity is examined using three dilution scenarios: (1) applying an entrainment rate (k_e) calculated from measurements of boundary layer height (BLH), (2) applying a dilution constant that scales according to the ratio of observed BLH and maximum BLH, and (3) using a constant dilution rate of either 2, 4, or 40 day^{-1}. Calculated dilution rates are derived in the supplement and shown in Fig. S1, and model results are shown in Figs. S2–S3. As in the base scenario, measured VOCs are constrained when calculating OH reactivity. The dilution rate of 4 day^{-1} used in the base scenarios is chosen based on the resultant agreement with several measured species including HCHO, glyoxal, glycolaldehyde, and PAN (Fig. S3). Further support of this is the good agreement between measured and model IEPOX when ISOPOOH is constrained using this rate constant (Fig. S4).

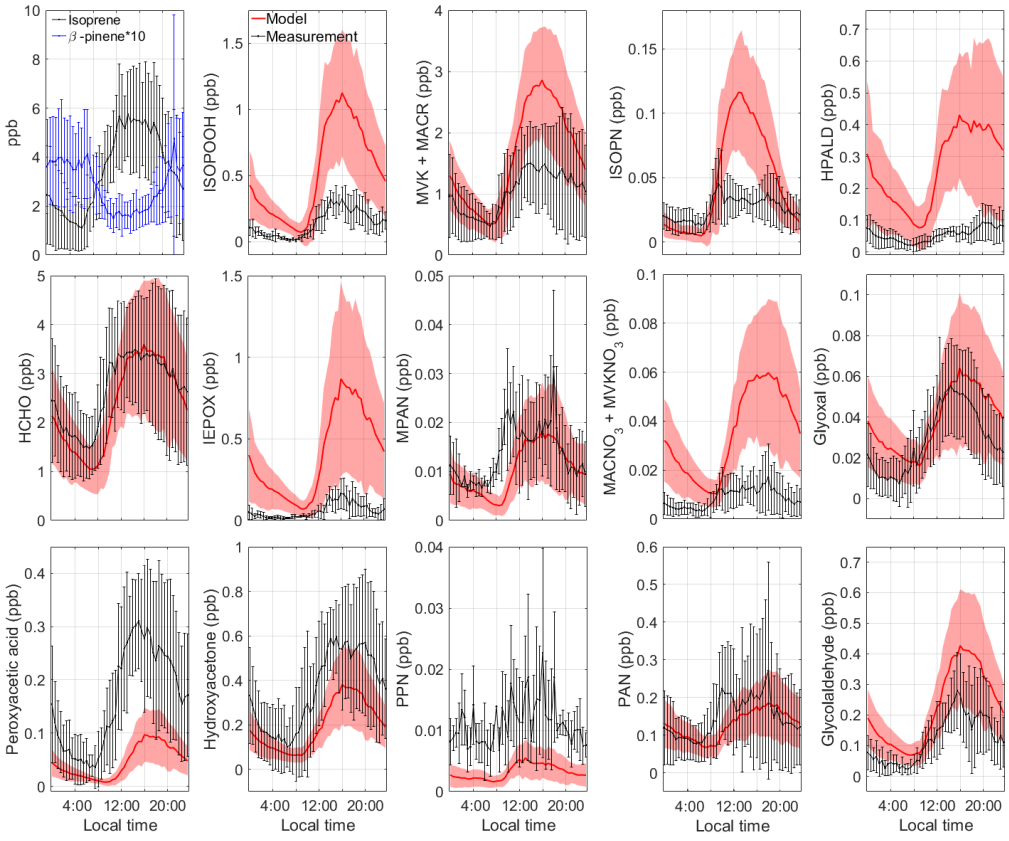

Figure 5. Average measured and modeled diurnal profiles of isoprene, β-pinene, and several measured oxidation products. Error bars and shaded area represent 1σ standard deviation of diurnal variability. For each species, model results are not included for points where measurements are missing.

In order for dilution alone to account for the low concentrations of first-generation oxidation products, extremely high dilution rates would need to be incorporated. For ISOPOOH, a constant rate of 40 day^{-1}, (roughly 5 times the photochemical loss rate) would be needed. Most importantly, when OVOCs are constrained, the assumed dilution scheme has very little effect on the model OH reactivity (Fig. S2), as measured species dominate total reactivity.

4 Discussion

While on average the model largely captures the absolute value of OH reactivity at SOAS (Fig. 1), there are small but significant differences (15 %) in the increase in total reactivity and reactivity from isoprene alone (slope of Fig. 4). While most measured species have uncertainties > 15 %, it is unlikely that all measured species are systematically low, suggesting this discrepancy is likely the result of unmeasured species. When given a constrained precursor, the model either reproduces or overpredicts the resulting oxidation products (Figs. 5, S4). As isoprene and its oxidation products are heavily constrained, we conclude that unmeasured primary species co-emitted with isoprene (and those species' oxidation products) are the likely source of this small discrepancy.

As observed daytime isoprene concentrations increase with temperature, the difference in slope also represents a temperature-dependent daytime missing reactivity. The temperature dependence observed at SOAS is greater than that observed by DiCarlo et al. (2004) and the dependence of monoterpene emissions, though it is important to note the different range of temperatures included in each set of observations (Fig. 6). Emissions which depend both on temperature and light are likely to have stronger net temperature dependence, as temperature increases with increasing solar radiation. Therefore, a portion of the total missing emissions could likely be characterized by both a light and temperature dependence.

Furthermore, the model is missing $\sim 1\,\mathrm{s}^{-1}$ reactivity that is temporally unrelated to the oxidation of isoprene and co-emitted species (intercept of Fig. 4). This is consistent with the diurnal variability of missing reactivity, with larger portions occurring at night and in the early morning (Fig. 2). Likely, missing nighttime reactivity is composed of a mixture of unmeasured primary emissions, unmeasured oxidation products, and long-lived unmeasured species mixed in

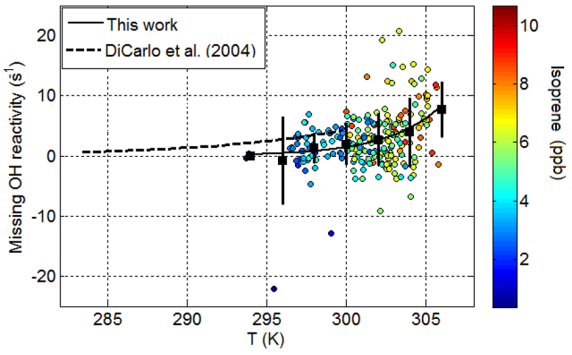

Figure 6. Daytime (10:00–16:00 LT) missing reactivity as a function of temperature and isoprene. Black squares represent 2° averages and standard deviations. All daytime points are fit according to the function $y = \alpha \cdot \exp(\beta(x - 293))$. The temperature dependence observed at SOAS ($\beta = 0.30$) is greater than that observed by DiCarlo et al. (2004) and the dependence of monoterpene emissions ($\beta = 0.11$).

from the residual layer. Xiong et al. (2015) show that 27 % of the early morning increase in ISOPN results from downward mixing from the residual layer during this campaign. Similarly, there may be unmeasured OH reaction partners stored in the nocturnal boundary layer that lead to an increase in OH reactivity upon breakup of the inversion. Like β-pinene, anthropogenic VOCs such as toluene and benzene are highest at night. However, these species were not unusually high during the 11–16 June period, which demonstrated the highest missing reactivity, and therefore unmeasured anthropogenic VOCs are unlikely the major source of discrepancy. Sesquiterpenes ($C_{15}H_{24}$) are another class of VOC which typically follow the emission patterns of monoterpenes. The total sesquiterpene emission rate from broadleaf trees is estimated to be ∼ 67 % of the emission rate of total monoterpenes in terms of total mass (Sakulyanontvittaya et al., 2008). Assuming a reaction rate with OH of β-caryophyllene, ∼ 200 ppt of sesquiterpenes would provide the 1 s^{-1} offset in reactivity temporally separated from isoprene.

Much like the previous work of Zannoni et al. (2016), we find good daytime agreement between measured and modeled reactivity above the forest canopy and that the majority of reactivity can be attributed to primary emissions. Using measurements of first- and later-generation OVOCs as a constraint on the amount of total unmeasured oxidation products, we find no evidence of substantial contributions of unmeasured OVOCs to above-canopy OH reactivity. This is in contrast to studies of Edwards et al. (2013) and Hansen et al. (2014), who showed that these species may contribute significantly to OH reactivity directly above the forest canopy. Varying amounts of intra-canopy oxidation are likely to result in these different conclusions, as secondary compounds will quickly become more important than the primary isoprene emissions at higher altitudes or farther downwind of the forest.

Based on measured OH concentrations, the measured concentrations of OVOCs suggest surprisingly little intra-canopy oxidation of primary VOCs at this site. Furthermore, advection does not appear to bring in processed isoprene emissions. Despite measuring ∼ 10 m above the forest canopy in a relatively homogeneous area, OH reactivity is primarily composed of measured primary species. Our model overpredicts concentrations of isoprene's first-generation oxidation products by at least a factor of 2. If these species and other OVOCs were not constrained by measurements, these overpredictions would lead to problematic conclusions about the speciation of reactivity. In the relationship of reactivity from isoprene to total reactivity, the modeled slope (1.22 ± 0.02) and measured slope (1.44 ± 0.02) would show no discrepancy. While the true observed missing contribution is small, it highlights the contribution from primary species whose oxidation may be important downwind.

5 Conclusions

In summary, when VOCs and their oxidation products are constrained to measured values, the discrepancies in the absolute value of measured and modeled OH reactivity are rarely significant at this site. Assuming that the RO_2 production rate can be represented by the VOC portion of OH reactivity (i.e., $VOC + OH -> RO_2$), this suggests that the RO_2 production rate from VOC oxidation is well captured by both measured OH reactivity and measured OVOCs/VOCs. Therefore, together with measurements of NO, both OH reactivity measurements and speciated OVOC/VOC measurements are well suited to characterize O_3 production rates at this site.

Small but significant discrepancies in the observed and calculated trend in OH reactivity with increasing isoprene suggest missing sources of reactive carbon. The model fails to capture a portion of reactivity that is temporally related to isoprene, as well as a portion unrelated to local isoprene oxidation. As isoprene oxidation products are heavily constrained and the model does not typically underestimate OVOCs, we propose that missing primary emissions and their oxidation products are likely candidates for both sources of reactive carbon. While these missing emissions do not lead to significant inconsistencies between measured and modeled OH reactivity, at larger total emissions, the trending discrepancy may lead to larger missing fractions of OH reactivity.

The speciation of this missing carbon source has air-quality-relevant implications. For example, though monoterpenes are much less abundant than isoprene, they can substantially effect SOA formation. Ayres et al. (2015) found that organic nitrate aerosol from NO_3 + monoterpenes is a substantial contribution to observed particulate matter at

this site, with an SOA molar yield of 23–44 %. In contrast, the comparable isoprene nitrate is primarily a gas-phase product. Through positive matrix factorization analysis of aerosol mass spectrometer measurements, Xu et al. (2015) found that monoterpene + NO_3 chemistry contributes 50 % to total nighttime organic aerosol formation at this site, whereas IEPOX-derived SOA constitutes 19–34 % total organic aerosol. Additionally, Su et al. (2016) cite aerosol uptake and condensed-phase reactivity as a possible explanation for the large discrepancy between observed and modeled ISOPOOH at this site, which implies a large loss of total carbon to the aerosol phase. While the magnitude of OH reactivity is well captured, continued efforts in speciated OVOC and VOC measurements are vital to fully understand the SOA contribution from various primary emissions.

6 Data availability

The SOAS research data used in this publication are available at http://esrl.noaa.gov/csd/field.html (2013, Southeast Nexus, SOAS Centreville Site).

The Supplement related to this article is available online at doi:10.5194/acp-16-9349-2016-supplement.

Acknowledgements. The authors would like to acknowledge contribution from all members of the SOAS science team. Funding was provided by US EPA "Science to Achieve Results (STAR) program" Grant 83540601. A. H. Goldstein and P. K. Misztal acknowledge support from EPA STAR Grant R835407. This research has not been subjected to any EPA review and therefore does not necessarily reflect the views of the Agency, and no official endorsement should be inferred. Additional funding was provided by NSF-grant AGS-1247421 and 1628530. J. Kaiser acknowledges support from NASA Headquarters under the NASA Earth and Space Science Fellowship Program – Grant NNX14AK97H.

Edited by: N. L. Ng
Reviewed by: two anonymous referees

References

Ayres, B. R., Allen, H. M., Draper, D. C., Brown, S. S., Wild, R. J., Jimenez, J. L., Day, D. A., Campuzano-Jost, P., Hu, W., de Gouw, J., Koss, A., Cohen, R. C., Duffey, K. C., Romer, P., Baumann, K., Edgerton, E., Takahama, S., Thornton, J. A., Lee, B. H., Lopez-Hilfiker, F. D., Mohr, C., Wennberg, P. O., Nguyen, T. B., Teng, A., Goldstein, A. H., Olson, K., and Fry, J. L.: Organic nitrate aerosol formation via NO^3 + biogenic volatile organic compounds in the southeastern United States, Atmos. Chem. Phys., 15, 13377–13392, doi:10.5194/acp-15-13377-2015, 2015.

Blanchard, C. L., Hidy, G., Tanenbaum, S., Edgerton, E., and Hartsell, B.: The southeastern aerosol research and characterization (SEARCH) study: Temporal trends in the PM and gas concentrations and composition, 1999–2010, JAPCA J. Air Waste Ma., 63, 247–259, doi:10.1080/10962247.2012.748523, 2013.

Crounse, J. D., McKinney, K. A., Kwan, A. J., and Wennberg, P. O.: Measurement of gas-phase hydroperoxides by chemical ionization mass spectrometry, Anal. Chem., 78, 6726–6732, doi:10.1021/ac0604235, 2006.

Crounse, J. D., Paulot, F., Kjaergaard, H. G., and Wennberg, P. O.: Peroxy radical isomerization in the oxidation of isoprene, Phys. Chem. Chem. Phys., 13, 13607–13613, doi:10.1039/c1cp21330j, 2011.

da Silva, G., Graham, C., and Wang, Z. F.: Unimolecular beta-Hydroxyperoxy Radical Decomposition with OH Recycling in the Photochemical Oxidation of Isoprene, Environ. Sci. Technol., 44, 250-256, doi:10.1021/es900924d, 2010.

DiCarlo, P., Brune, W. H., Martinez, M., Harder, H., Lesher, R., Ren, X., Thornberry, T., Carroll, M., Young, V., Shepson, P., Riemer, D., Apel, E., and Campbell, C.: Missing OH reactivity in a forest: evidence for unknown reactive biogenic VOCs, Science, 304, 722–725, doi:10.1126/science.1094392, 2004.

DiGangi, J. P., Boyle, E. S., Karl, T., Harley, P., Turnipseed, A., Kim, S., Cantrell, C., Maudlin III, R. L., Zheng, W., Flocke, F., Hall, S. R., Ullmann, K., Nakashima, Y., Paul, J. B., Wolfe, G. M., Desai, A. R., Kajii, Y., Guenther, A., and Keutsch, F. N.: First direct measurements of formaldehyde flux via eddy covariance: implications for missing in-canopy formaldehyde sources, Atmos. Chem. Phys., 11, 10565–10578, doi:10.5194/acp-11-10565-2011, 2011.

Edwards, P. M., Evans, M. J., Furneaux, K. L., Hopkins, J., Ingham, T., Jones, C., Lee, J. D., Lewis, A. C., Moller, S. J., Stone, D., Whalley, L. K., and Heard, D. E.: OH reactivity in a South East Asian tropical rainforest during the Oxidant and Particle Photochemical Processes (OP3) project, Atmos. Chem. Phys., 13, 9497–9514, doi:10.5194/acp-13-9497-2013, 2013.

Feiner, P. A., Brune, W. H., Miller, D. O., Zhang, L., Cohen, R. C., Romer, P., Goldstein, A. H., Keutsch, F. N., Skog, K. M., Wennberg, P. O., Nguyen, T. B., Teng, A. P., DeGouw, J. A., Koss., A., Wild, R. J., Brown. S. S., Guenther, A., Edgerton, E. S., Baumann, K., and Fry, J. L.: Testing Atmospheric Oxidation in an Alabama Forest, J. Atmos. Sci., submitted, 2016.

Fuchs, H., Dubé, W. P., Lerner, B. M., Wagner, N. L., Williams, E. J., and Brown, S. S.: A Sensitive and Versatile Detector for Atmospheric NO_2 and NO_x Based on Blue Diode Laser Cavity Ring-Down Spectroscopy, Environ. Sci. Technol., 43, 7831–7836, doi:10.1021/es902067h, 2009.

Gilman, J. B., Burkhart, J. F., Lerner, B. M., Williams, E. J., Kuster, W. C., Goldan, P. D., Murphy, P. C., Warneke, C., Fowler, C., Montzka, S. A., Miller, B. R., Miller, L., Oltmans, S. J., Ryerson, T. B., Cooper, O. R., Stohl, A., and de Gouw, J. A.: Ozone variability and halogen oxidation within the Arctic and sub-Arctic springtime boundary layer, Atmos. Chem. Phys., 10, 10223–10236, doi:10.5194/acp-10-10223-2010, 2010.

Guenther, A. B., Jiang, X., Heald, C. L., Sakulyanontvittaya, T., Duhl, T., Emmons, L. K., and Wang, X.: The Model of Emissions of Gases and Aerosols from Nature version 2.1 (MEGAN2.1): an extended and updated framework for modeling biogenic emis-

sions, Geosci. Model Dev., 5, 1471–1492, doi:10.5194/gmd-5-1471-2012, 2012.

Hansen, R. F., Griffith, S. M., Dusanter, S., Rickly, P. S., Stevens, P. S., Bertman, S. B., Carroll, M. A., Erickson, M. H., Flynn, J. H., Grossberg, N., Jobson, B. T., Lefer, B. L., and Wallace, H. W.: Measurements of total hydroxyl radical reactivity during CABINEX 2009 – Part 1: field measurements, Atmos. Chem. Phys., 14, 2923–2937, doi:10.5194/acp-14-2923-2014, 2014.

Hidy, G. M., Blanchard, C. L., Baumann, K., Edgerton, E., Tanenbaum, S., Shaw, S., Knipping, E., Tombach, I., Jansen, J., and Walters, J.: Chemical climatology of the southeastern United States, 1999–2013, Atmos. Chem. Phys., 14, 11893–11914, doi:10.5194/acp-14-11893-2014, 2014.

Hottle, J. R., Huisman, A. J., DiGangi, J. P., Kammrath, A., Galloway, M. M., Coens, K. L., and Keutsch, F. N.: A laser induced fluorescence-based instrument for in-situ measurements of atmospheric formaldehyde, Environ. Sci. Technol., 43, 790–795, doi:10.1021/es801621f, 2008.

Huisman, A. J., Hottle, J. R., Coens, K. L., DiGangi, J. P., Galloway, M. M., Kammrath, A., and Keutsch, F. N.: Laser-induced phosphorescence for the in situ detection of glyoxal at part per trillion mixing ratios, Anal. Chem., 80, 5884–5891, doi:10.1021/ac800407b, 2008.

Jenkin, M., Saunders, S., and Pilling, M.: The tropospheric degradation of volatile organic compounds: A protocol for mechanism development, Atmos. Environ., 31, 81–104, doi:10.1016/S1352-2310(96)00105-7, 1997.

Jordan, A., Haidacher, S., Hanel, G., Hartungen, E., Herbig, J., Märk, L., Schottkowsky, R., Seehauser, H., Sulzer, P., and Märk, T.: An online ultra-high sensitivity proton-transfer-reaction mass-spectrometer combined with switchable reagent ion capability (PTR + SRI − MS), Int. J. Mass Spectrom., 286, 32–38, 2009.

Kim, S., Karl, T., Helmig, D., Daly, R., Rasmussen, R., and Guenther, A.: Measurement of atmospheric sesquiterpenes by proton transfer reaction-mass spectrometry (PTR-MS), Atmos. Meas. Tech., 2, 99–112, doi:10.5194/amt-2-99-2009, 2009.

Kim, S., Guenther, A., Karl, T., and Greenberg, J.: Contributions of primary and secondary biogenic VOC tototal OH reactivity during the CABINEX (Community Atmosphere-Biosphere INteractions Experiments)-09 field campaign, Atmos. Chem. Phys., 11, 8613–8623, doi:10.5194/acp-11-8613-2011, 2011.

Kovacs, T. A. and Brune, W. H.: Total OH Loss Rate Measurement, J. Atmos. Chem., 39, 105–122, doi:10.1023/A:1010614113786, 2001.

Lee, L., Teng, A. P., Wennberg, P. O., Crounse, J. D., and Cohen, R. C.: On rates and mechanisms of OH and O_3 reactions with isoprene-derived hydroxy nitrates, J. Phys. Chem. A, 118, 1622–1637, doi:10.1021/jp4107603, 2014.

Mao, J., Ren, X., Brune, W. H., Olson, J. R., Crawford, J. H., Fried, A., Huey, L. G., Cohen, R. C., Heikes, B., Singh, H. B., Blake, D. R., Sachse, G. W., Diskin, G. S., Hall, S. R., and Shetter, R. E.: Airborne measurement of OH reactivity during INTEX-B, Atmos. Chem. Phys., 9, 163–173, doi:10.5194/acp-9-163-2009, 2009.

Nguyen, T. B., Crounse, J. D., Teng, A. P., St. Clair, J. M., Paulot, F., Wolfe, G. M., and Wennberg, P. O.: Rapid deposition of oxidized biogenic compounds to a temperate forest, P. Natl. Acad. Sci. USA, 112, E392–E401, doi:10.1073/pnas.1418702112, 2015.

Nölscher, A. C., Butler, T., Auld, J., Veres, P., Muñoz, A., Taraborrelli, D., Vereecken, L., Lelieveld, J., and Williams, J.: Using total OH reactivity to assess isoprene photooxidation via measurement and model, Atmos. Environ., 89, 453–463, doi:10.1016/j.atmosenv.2014.02.024, 2014.

Paulot, F., Crounse, J. D., Kjaergaard, H. G., Kroll, J. H., Seinfeld, J. H., and Wennberg, P. O.: Isoprene photooxidation: new insights into the production of acids and organic nitrates, Atmos. Chem. Phys., 9, 1479–1501, doi:10.5194/acp-9-1479-2009, 2009.

Peeters, J. and Müller, J. F.: HO_x radical regeneration in isoprene oxidation via peroxy radical isomerisations. II: experimental evidence and global impact, Phys. Chem. Chem. Phys., 12, 14227–14235, doi:10.1039/C0CP00811G, 2010.

Rivera-Rios, J. C., Nguyen, T. B., Crounse, J. D., Jud, W., St. Clair, J. M., Mikoviny, T., Gilman, J. B., Lerner, B. M., Kaiser, J. B., de Gouw, J., Wisthaler, A., Hansel, A., Wennberg, P. O., Seinfeld, J. H., and Keutsch, F. N.: Conversion of hydroperoxides to carbonyls in field and laboratory instrumentation: Observational bias in diagnosing pristine versus anthropogenically controlled atmospheric chemistry, Geophys. Res. Lett., 41, 8645–8651, doi:10.1002/2014GL061919, 2014.

Roberts, J. M., Flocke, F., Stroud, C. A., Hereid, D., Williams, E. J., Fehsenfeld, F. C., Brune, W., Martinez, M., and Harder, H.: Ground-based measurements of peroxycarboxylic nitric anhydrides (PANs) during the 1999 Southern Oxidant Study Nahville Intensive, J. Geophys. Res., 107, 4554, doi:10.1029/2001JD000947, 2002.

Sakulyanontvittaya, T., Duhl, T., Wiedinmyer, C., Helmig, D., Matsunaga, S., Potosnak, M., Milford, J., and Guenther, A.: Monoterpene and sesquiterpene emission estimates for the United States, Environ. Sci. Technol., 42, 1623–1629, 2008.

Saunders, S. M., Jenkin, M. E., Derwent, R. G., and Pilling, M. J.: Protocol for the development of the Master Chemical Mechanism, MCM v3 (Part A): tropospheric degradation of non-aromatic volatile organic compounds, Atmos. Chem. Phys., 3, 161–180, doi:10.5194/acp-3-161-2003, 2003.

Sinha, V., Williams, J., Crowley, J. N., and Lelieveld, J.: The Comparative Reactivity Method – a new tool to measure total OH Reactivity in ambient air, Atmos. Chem. Phys., 8, 2213–2227, doi:10.5194/acp-8-2213-2008, 2008.

St. Clair, J. M., McCabe, D. C., Crounse, J. D., Steiner, U., and Wennberg, P. O.: Chemical ionization tandem mass spectrometer for the in situ measurement of methyl hydrogen peroxide, Rev. Sci. Instrum., 81, 094102–094106, 2010.

St. Clair, J. M., Spencer, K. M., Beaver, M. R., Crounse, J. D., Paulot, F., and Wennberg, P. O.: Quantification of hydroxyacetone and glycolaldehyde using chemical ionization mass spectrometry, Atmos. Chem. Phys., 14, 4251–4262, doi:10.5194/acp-14-4251-2014, 2014.

St. Clair, J. M., Rivera, J. C., Crounse, J. D., Knap, H. C., Bates, K. H., Teng, A. P., Jørgensen So., Kjaergaard, H. G., Keutsch, F. N., and Wennberg, P. O.: Kinetics and Products of the Reaction of the First-Generation Isoprene Hydroxy Hydroperoxide (ISOPOOH) with OH, J. Phys. Chem. A., 120, 1441–1451, doi:10.1021/acs.jpca.5b06532, 2015.

Su, L., Patton, E. G., Vilà-Guerau de Arellano, J., Guenther, A. B., Kaser, L., Yuan, B., Xiong, F., Shepson, P. B., Zhang, L., Miller, D. O., Brune, W. H., Baumann, K., Edgerton, E., Weinheimer, A., Misztal, P. K., Park, J.-H., Goldstein, A. H., Skog, K. M.,

Keutsch, F. N., and Mak, J. E.: Understanding isoprene photooxidation using observations and modeling over a subtropical forest in the southeastern US, Atmos. Chem. Phys., 16, 7725–7741, doi:10.5194/acp-16-7725-2016, 2016.

Thirumalai, K., Singh, A., and Ramesh, R.: A MATLAB code to perform weighted linear regression with (correlated or uncorrelated) errors in bivariate data, J. Geol. Soc. India, 77, 377–380, doi:10.1007/s12594-011-0044-1, 2011.

Wild, R. J., Edwards, P. M., Dubé, W. P., Baumann, K., Edgerton, E. S., Quinn, P. K., Roberts, J. M., Rollins, A. W., Veres, P. R., Warneke, C., Williams, E. J., Yuan, B., and Brown, S. S.: A Measurement of Total Reactive Nitrogen, NO_y, together with NO_2, NO, and O_3 via Cavity Ring-down Spectroscopy, Environ. Sci. Technol., 48, 9609–9615, doi:10.1021/es501896w, 2014.

Wolfe, G. M. and Thornton, J. A.: The Chemistry of Atmosphere-Forest Exchange (CAFE) Model – Part 1: Model description and characterization, Atmos. Chem. Phys., 11, 77–101, doi:10.5194/acp-11-77-2011, 2011.

Wolfe, G. M., Crounse, J. D., Parrish, J. D., St. Clair, J. M., Beaver, M. R., Paulot, F., Yoon, T. P., Wennberg, P. O., and Keutsch, F. N.: Photolysis, OH reactivity and ozone reactivity of a proxy for isoprene derived hydroperoxyenals (HPALDs), Phys. Chem. Chem. Phys., 14, 7276–7286, doi:10.1039/c2cp40388a, 2012.

Xiong, F., McAvey, K. M., Pratt, K. A., Groff, C. J., Hostetler, M. A., Lipton, M. A., Starn, T. K., Seeley, J. V., Bertman, S. B., Teng, A. P., Crounse, J. D., Nguyen, T. B., Wennberg, P. O., Misztal, P. K., Goldstein, A. H., Guenther, A. B., Koss, A. R., Olson, K. F., de Gouw, J. A., Baumann, K., Edgerton, E. S., Feiner, P. A., Zhang, L., Miller, D. O., Brune, W. H., and Shepson, P. B.: Observation of isoprene hydroxynitrates in the southeastern United States and implications for the fate of NO_x, Atmos. Chem. Phys., 15, 11257–11272, doi:10.5194/acp-15-11257-2015, 2015.

Xu, L., Guo, H., Boyd, C. M., Klein, M., Bougiatioti, A., Cerully, K. M., Hite, J. R., Isaacman-VanWerts, G., Kreisberg, N. M., Knote, C., Olson, K., Koss, A., Goldstein, A. H., Hering, S. V., de Gouw, J., Baumann, K., Lee, S.-H., Nenes, A., Weber, R. J., and Ng, N. L.: Effects of anthropogenic emissions on aerosol formation from isoprene and monoterpenes in the Southeastern United States, P. Natl. Acad. Sci. USA, 112, 37–42, doi:10.1073/pnas.1417609112, 2015.

York, D., Evensen, N. M., Marinez, M. L., and Delgado, J. D. B.: Unified equations for the slope, intercept, and standard errors of the best straight line, Am. J. Phys., 72, 367–375, doi:10.1119/1.1632486, 2004.

Zannoni, N., Gros, V., Lanza, M., Sarda, R., Bonsang, B., Kalogridis, C., Preunkert, S., Legrand, M., Jambert, C., Boissard, C., and Lathiere, J.: OH reactivity and concentrations of biogenic volatile organic compounds in a Mediterranean forest of downy oak trees, Atmos. Chem. Phys., 16, 1619–1636, doi:10.5194/acp-16-1619-2016, 2016.

Supplement of Atmos. Chem. Phys., 16, 9349–9359, 2016
http://www.atmos-chem-phys.net/16/9349/2016/
doi:10.5194/acp-16-9349-2016-supplement

Atmospheric Chemistry and Physics
Open Access
EGU

Supplement of

Speciation of OH reactivity above the canopy of an isoprene-dominated forest

J. Kaiser et al.

Correspondence to: J. Kaiser (jkaiser@seas.harvard.edu)

Supplemental Information

1 Missing data interpolation

Overall, the SOAS dataset is very complete with very few gaps in observations; however; in order to constrain the model, all gaps must be filled. If the period of missing data is less than 2 hours, a cubic interpolation of the entire time series is used to replace the missing points. If the data gap is larger, the missing points are replaced in one of the following ways:

(1) For species with no clear diurnal cycle, the measurement average is used. This primarily applies to anthropogenic VOCs with low concentrations (i.e. xylenes).

(2) For species that exhibit clear, consistent diurnal cycle but may have entire days with missing data, the diurnal average is used. This primarily applies to OVOCs (i.e. IEPOX).

(3) For isoprene, missing data is filled using a standard least squares regression of temperature and measured mixing ratios for all measurement points (r^2=0.68). Similarly, standard least squares regression of isoprene and MVK+MACR is used to fill missing MVK+MACR data (r^2=0.55).

(4) For NO, NO_2, and O_3, missing data were filled using measurements from an instrument in a nearby trailer. For HNO_3, a standard least squares regression between ground and tower observations is used to fill data gaps (r^2=0.51).

For all figures and analysis, model outputs are not included for time periods during with gaps in OH, OH reactivity, or isoprene measurements. Results are also not included for 28 June, 9 July, and 10 July are also excluded as PTR-MS and GC isoprene measurements could not be reconciled on these days.

2 Sensitivity to dilution rate

Ideally, a time-dependent dilution constant would be applied that represents mixing in of the residual layer, strong boundary layer growth throughout the morning, a maximum boundary

layer height in the afternoon boundary layer height, and little vertical mixing at night. The entrainment rate into the boundary layer is given by:

$$\text{Entrainment Rate} = \frac{v}{BLH}([X]_{FT} - [X]_{BL}) \quad (1)$$

Where *BLH* is the boundary layer height, $[X]_{BLH}$ and $[X]_{FT}$ refer to the concentration of a given species in the boundary layer and the free troposphere, and *v* is the entrainment velocity. The entrainment rate constant (k_e) is *v/BLH*. As *v* is equivalent to the change of BLH with time, we arrive at:

$$k_e = \frac{1}{BLH} d[BLH]/dt \quad (2)$$

Integrating yields:

$$k_e = \ln(\frac{BLH_{t1}}{BLH_{t2}})/dt \quad (3)$$

The calculated k_e from BLH measurements is very sensitive to measurement noise. Therefore, we calculate k_e by taking a smoothed version of the diurnal average BLH measurement acquired by ceilometer. Dilution is ignored where $k_e<0$.

As OH reactivity is dominated by measured species, k_{dil} has minimal impact on the calculated OH reactivity. In the relationship between total OH reactivity and reactivity from isoprene, the model slope and intercept are both slightly dependent on the dilution rate (Table S1). However, under nearly all model scenarios, the slope and intercept are slightly underestimated. The intercept for the entrainment scenario is higher than the measurement case because of the inaccurately high calculated nighttime OVOC concentrations (Fig. S3). The more accurate representations of dilution are consistent with the primary conclusions: (1) the contribution to total OH reactivity from unmeasured, unconstrained OVOCs is small (2) there is a small but significant discrepancy in the relationship between observed and modeled total reactivity and reactivity from isoprene alone.

3 Sensitivity to OH and HO_2 concentrations

A full discussion of the OH and HO_2 budget during this campaign can be found in Feiner et al. (2016). Importantly, our model concentrations are similar to theirs, and have minimal impact on OH reactivity and OVOC concentrations (Fig. S5).

Table S1. Least squares linear fit for model OH reactivity as a function of the OH reactivity from isoprene alone under different assumed dilution rates.

Dilution Rate	**Slope**	**Intercept (s^{-1})**
Calculated entrainment rate	1.15	7.43
Scaled to BLH	1.22	6.08
2 day^{-1}	1.22	6.04
4 day^{-1}	1.22	5.36
40 day^{-1}	1.17	4.65
Measurement	1.44	6.43

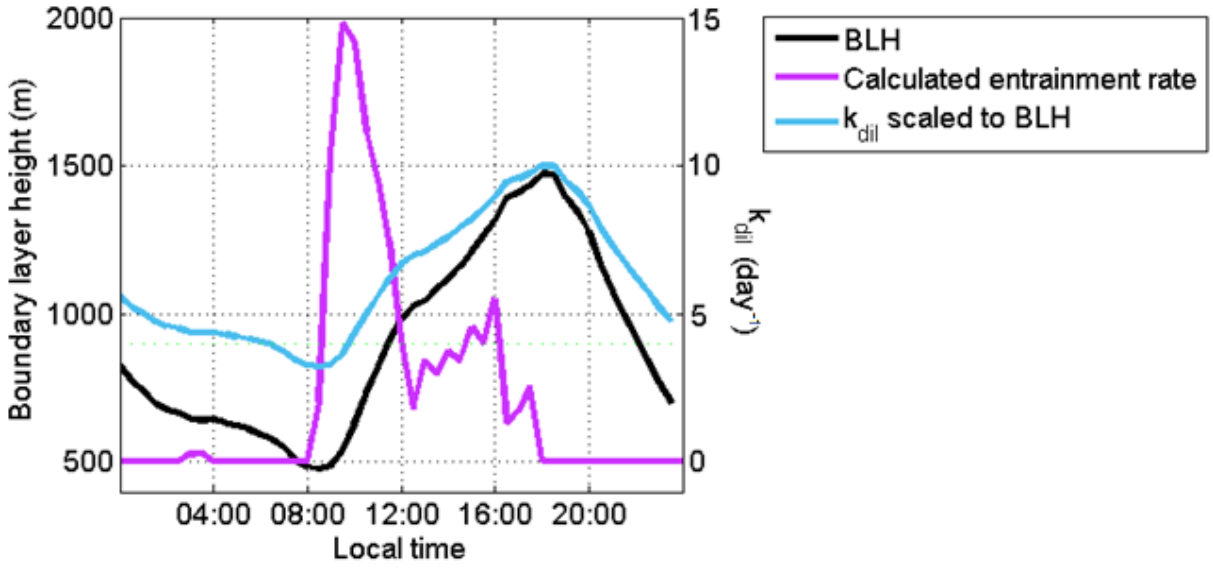

Figure S1. Diurnal average of boundary layer, smoothed over 2.5 hours, resultant dilution constant calculated according to Eq. 2, and dilution constant calculated from the ratio of BLH to maximum observed BLH.

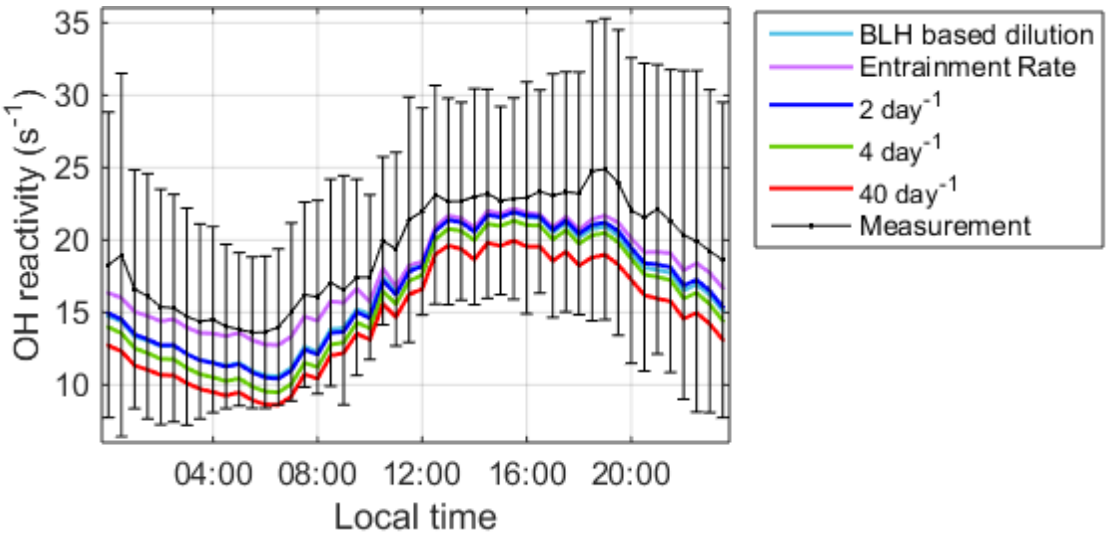

Figure S2. Sensitivity analysis for variability in the assumed dilution rate for OH reactivity. All measured species are constrained in this analysis. Error bars represent 1 σ diurnal variability in measurements. For clarity, diurnal variability is not shown in model results.

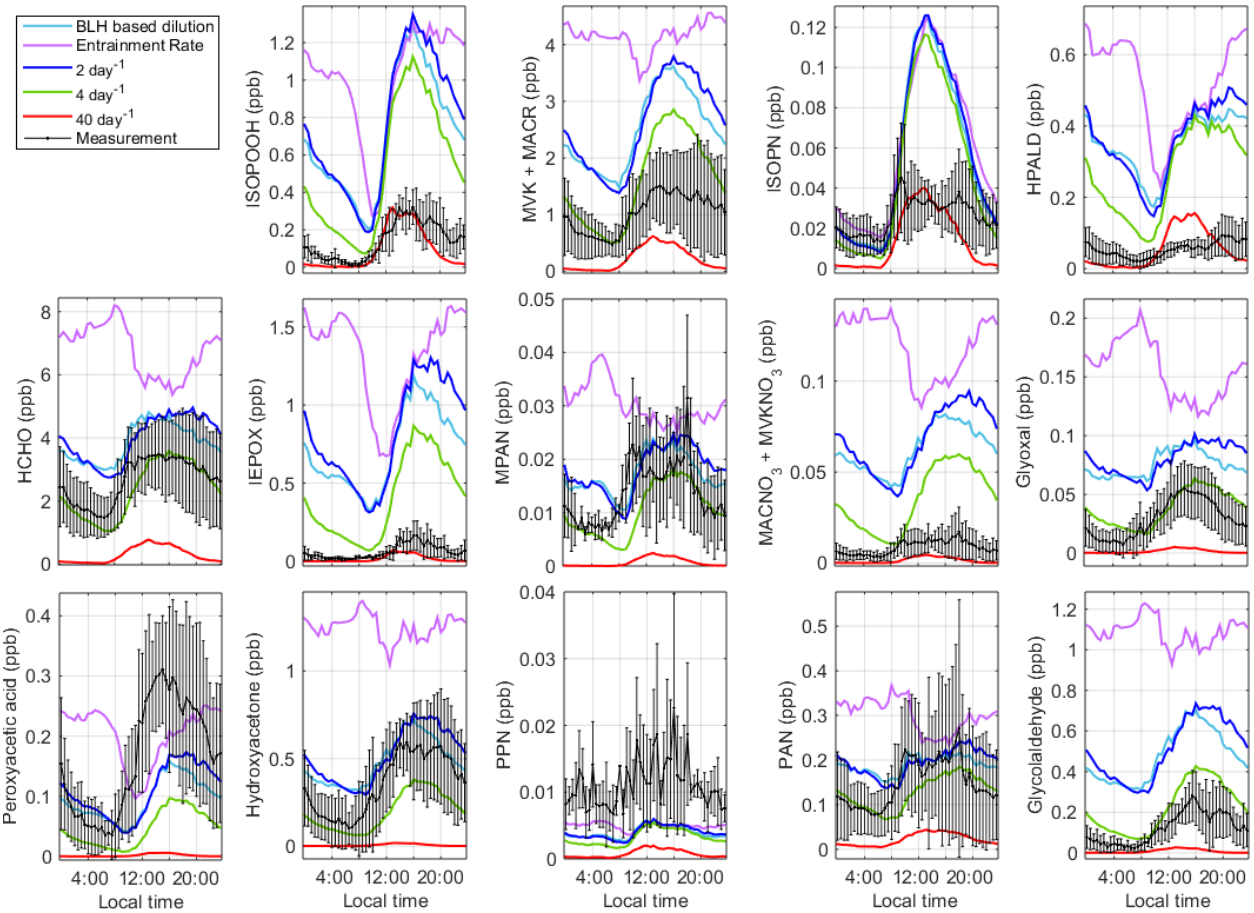

Figure S3. Sensitivity analysis for variability in the assumed dilution rate for OVOCs. Error bars represent 1 σ diurnal variability in measurements. For clarity, diurnal variability is not shown in model results. For each species, model results are not included for points where measurements are missing.

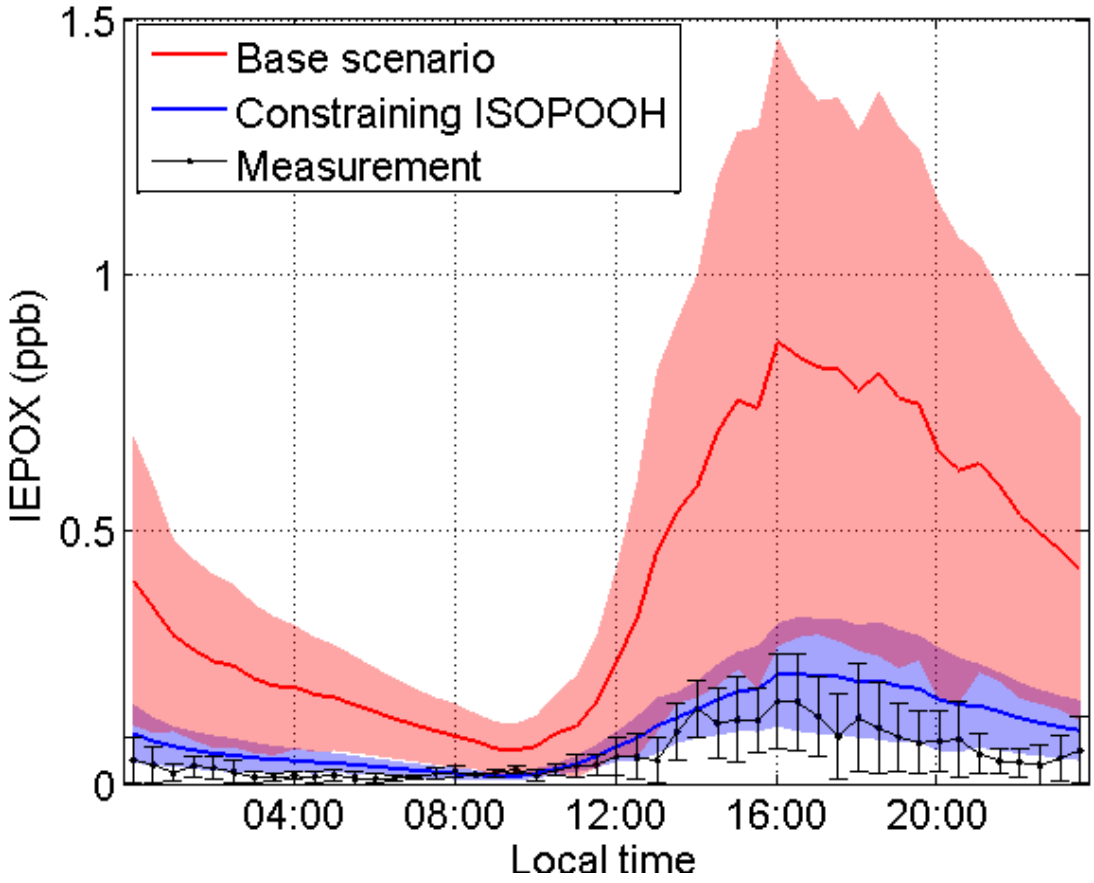

Figure S4. Comparison of measured and modeled concentrations of IEPOX with and without ISOPOOH constrained. Error bars and shaded area represent 1σ standard deviation of diurnal variability.

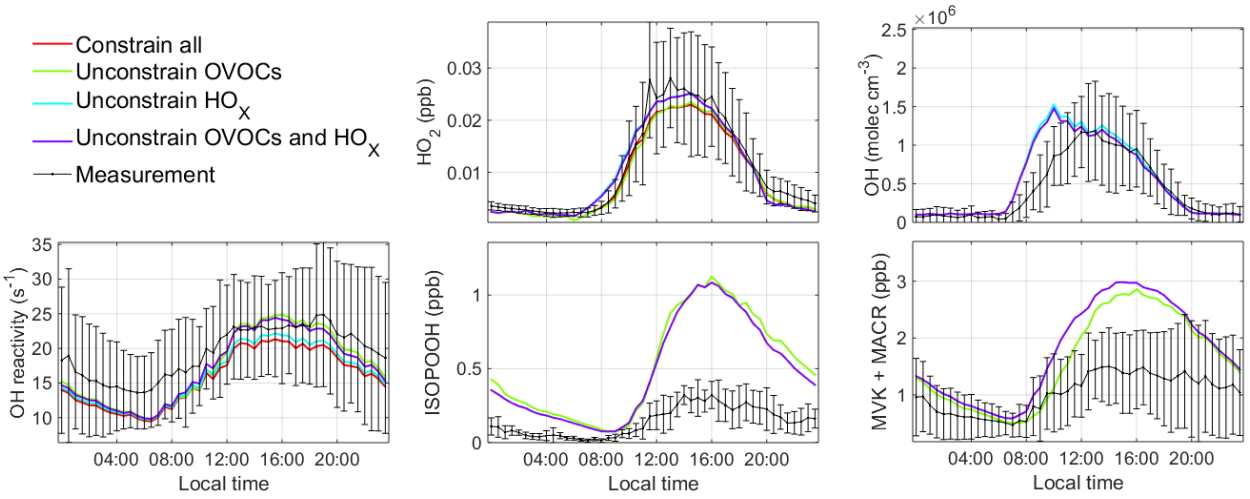

Figure S5. Model results of constraining or calculating OVOCs and HO_X on OH reactivity, HO_X, and specified OVOCs. Error bars on the measurement represent 1 σ diurnal variability. All scenarios use a constant dilution rate of 4 day^{-1}.